Synthesis and comparative chemistry of the early–late transition metal heterobimetallacycles $CpCp'Ta(CH_2)_2Ir(CO)(L)$ and their main-group element–late transition metal analogues $R_2P(CH_2)_2Ir(CO)(L)$

Michael J. Hostetler, Matthew D. Butts and Robert G. Bergman*
Department of Chemistry, University of California, Berkeley, CA 94720 (USA)

Abstract

The synthesis of two tantalum–iridium heterodinuclear complexes formed by the reaction of $CpCp'Ta(CH_2)(CH_3)$ with $IndIr(CO)_2$ is presented (Cp' = Cp (**1a**); indenyl (**1b**)). An X-ray diffraction study of the compound $(Ind)CpTa(CH_2)_2Ir(CO)_2$ was performed: the $Ta(CH_2)_2Ir$ ring is planar and the Ta–Ir bond length is 2.858(1) Å. These compounds react with phosphines to form substitution and addition products. The crystal structure of the PEt_3 adduct $Cp_2Ta(CH_2)_2Ir(CO)_2(PEt_3)$ (**2**) is presented; the geometry about the iridium center of **2** is midway between a square-based pyramid and a trigonal bipyramid, and the Ta–Ir bond length is 2.881(1) Å. Compound **1a** reacts with MeI to form the six-coordinate iridium oxidative addition product $Cp_2Ta(CH_2)_2Ir(CO)_2(CH_3)I$. The compound $Cp_2Ta(CH_2)_2Ir(CO)(PPh_3)$ (**3**) reacts with MeI in an analogous manner ($k_{2nd} = 7.61 \pm 0.43$ M^{-1} s^{-1}, THF, −5 °C). In order to assess the effect of the early metal on the chemistry at the late transition metal center, the chelating phosphorus ylide analogues $R_2P(CH_2)_2Ir(CO)(PPh_3)$ (R = Ph (**6a**), Me (**6b**)) were synthesized by treatment of the ylide anion, $R_2P(CH_2)_2Li$ with Vaska's complex $(PPh_3)_2Ir(CO)Cl$. An X-ray diffraction study performed on **6a** showed that the $Ir(CH_2)_2P$ metallacycle, in contrast to that of the Ta–Ir compounds, is non-planar. The ylide P–Ir distance (2.746(1) Å) is beyond bonding interaction. Compounds **6a** ($k_{2nd} = 7.55 \pm 0.30$ M^{-1} s^{-1}, THF, −5 °C) and **6b** ($k_{2nd} = 17.9 \pm 1.4$ M^{-1} s^{-1}, THF, −5 °C) react with CH_3I in a fashion analogous to that of the Ta–Ir complexes. Unlike compound **3**, both **6a** and **6b** are highly fluxional in solution due to the dissociation of the PPh_3 ligand from the Ir center. In addition, the metallacycle undergoes rapid ring inversion in solution, even at −90 °C. These studies suggest the early metal fragment can act as an electron sink and source for the late transition metal fragment through a direct Ta–Ir bond interaction.

Introduction

The development of generalized routes to the synthesis of early–late transition metal heterobimetallic (ELHB) compounds and the study of their reactivity, both stoichiometric and catalytic, is an intense area of research [1–6]. The co-activation of a substrate, such as carbon monoxide, by binding the molecule to both metals is one of the driving forces of this area of organometallic chemistry. However, even the simple catalytic behavior of these complexes has rarely been studied [7, 8]. Recently we reported that $Cp_2Ta(CH_2)_2Ir(CO)_2$ (**1a**) [9] catalyzes the hydrogenation and hydrosilation of alkenes and thus undertook a detailed mechanistic study of both of these reactions [10].

However, we discovered that we did not understand the interplay between the early and late transition metals. Therefore a study of the reactivity of an ELHB complex relative to that of its non-metal analogue (formed by substituting a non-metal fragment with similar steric and electronic properties for the early metal portion of an ELHB complex) was initiated in the hope of identifying the structural and chemical properties unique to this interaction.

We chose to replace the Cp_2Ta group by Ph_2P and Me_2P moieties because ylide compounds such as $Ph_3P{=}CH_2$ are isoelectronic with Ta carbenes [11]. In addition, phosphorus compounds often exhibit chemical reactivity similar to that of their Ta analogues [12, 13]. Ta and P also exhibit comparable oxophilicity and Lewis acidic properties. We now wish to report the results of our investigations on the structural, spectroscopic and chemical similarities (and differences) of the two

*Author to whom correspondence should be addressed.

0020-1693/92/$5.00

sets of compounds $Cp_2Ta(CH_2)_2Ir(CO)(L)$ and $R_2P(CH_2)_2Ir(CO)(L)$.

Experimental

General

Unless otherwise noted, all reactions and manipulations were performed in dry glassware under a nitrogen atmosphere in a Vacuum Atmospheres 553-2 drybox equipped with an M6-40-1H Dri-train or using standard Schlenk techniques. 'Glass bombs' refer to cylindrical, medium-walled Pyrex vessels joined to Kontes K-826510 high-vacuum teflon stopcocks. Unless otherwise noted, all reactions were performed at room temperature.

Benzene, toluene, Et_2O, pentane and THF were distilled from sodium/benzophenone, and methylene chloride was distilled from CaH_2. Methyl iodide was distilled from $CaCl_2$ and stored over a copper wire under nitrogen in the absence of light. $Cp_2Ta(CH_2)(CH_3)$ was prepared according to a literature procedure [11]. The synthesis of compounds $Cp_2Ta(CH_2)_2Ir(CO)(PPh_3)$ (**3**), $Ph_2P(CH_2)_2Ir(CO)(PPh_3)$ (**6a**) and $Me_2P(CH_2)_2Ir(CO)(PPh_3)$ (**6b**) are reported in a separate paper [10]. Unless otherwise noted, all other reagents were used as received from commercial suppliers.

$Cp_2Ta(CH_2)_2Ir(CO)_2$ (1a)

Method A. A solution of 500 mg of $(Ind)Ir(C_2H_4)_2$ [14] (1.37 mmol) in 20 ml of Et_2O was placed in a 100 ml glass bomb. The bomb was brought out of the box, frozen at 77 K and degassed once. To this frozen solution was added 410 torr of CO (8.54 mmol). The bomb was covered with aluminum foil to prevent decomposition of the light-sensitive $(Ind)Ir(CO)_2$ product. After standing for 2 h at room temperature, the bomb was brought back into the dry box. With the lights dimmed, the $(Ind)Ir(CO)_2$ solution was poured into a stirred solution of 480 mg of $Cp_2Ta(CH_2)(CH_3)$ (1.41 mmol) in 50 ml of diethyl ether in a 200 ml round bottom flask wrapped in aluminum foil. The solution was stirred for 16 h and then the solvent was removed under vacuum. The orange residue was washed with 3 ml aliquots of Et_2O until the color of the wash solution was pale yellow. The yellow residue was dissolved in a minimum amount of benzene and crystallized by vapor diffusion of pentane into the benzene solution at 20 °C for 1 day and then −30 °C for another day. The overall yield of the yellow crystalline **1a** was 700 mg (82%).

Method B. To a stirred solution of $IrCl(CO)_2(NH_2tol)$ [15] (50 mg, 128 μmol) in 20 ml of THF was added a solution of 43.4 mg of $Cp_2Ta(CH_2)(CH_3)$ (128 μmol) and 51 mg of $KN(TMS)_2$ (256 μmol) in 20 ml of THF. After stirring the solution for 2 h the solvent was removed under vacuum. The purple residue was washed with 2×20 ml of pentane to remove excess $KN(TMS)_2$. The remaining powder was dissolved in 5 ml of benzene and filtered through a pad of celite. Crystallization was effected as above to yield 60 mg (80%) of **1a**.

Method C. As in method B, except that no $KN(TMS)_2$ was added and the reaction was stirred for 1 day. Yield 18%, m.p. 233 °C (dec). ^1H NMR (C_6D_6): δ 5.28 (s, 4H, CH_2), 4.44 (s, 10H, Cp); (THF-d_8): δ 5.30 (s, 10H, Cp), 5.23 (s, 4H, CH_2). $^{13}C\{^1H\}$ NMR (THF-d_8): δ 192.4 (s, CO), 108.9 (s, $J(CH) = 135.6$, CH_2), 100.0 (s, $J(CH) = 178.2$, 6.7, Cp); IR (THF-d_8): $\nu(CO) = 2008$, 1946 cm^{-1}. UV–Vis (THF) (nm): 282 ($\epsilon = 12\,400$ cm^{-1} M^{-1}), 354 (3170), 404 (4250), 456 (768). MS (EI): 588 (M^+), 560 ($M^+ - CO$), 532 ($M^+ - 2\,CO$). HR-MS (EI): *m/e* calc. for $C_{14}H_{14}O_2TaIr$, 588.0100; found, 588.0103.

$Cp_2Ta(CD_2)_2Ir(CO)_2$ (1a-d_4)

A solution of 20 mg of $(Ind)Ir(C_2H_4)$ (55 μmol) in 1.6 ml of C_6D_6 was added to a 5 ml glass bomb. The solution was frozen at 77 K and degassed. To this was added 400 torr of CO (366 μmol). The bomb was wrapped in aluminum foil and the solution thawed. After the solution was shaken by hand for 10 min the bomb was brought back into the dry box. The solution was added to a vial containing 19 mg of $Cp_2Ta(CD_2)(CD_3)$ [10] (55 μmol) and stirred for 10 min. A ^1H NMR spectrum was taken of 0.5 ml of this solution. Free indene, monodeuterated at the allylic position, was seen (the resonance at 3.58 ppm integrated to only one hydrogen). In addition, no resonance was seen in the spectrum for the μ-CH_2 groups of **1a**, indicating complete deuteration. ^2H NMR (C_6H_6): δ 5.22.

$Cp(Ind)TaMe_2^+BF_4^-$

(1) *Preparation of crude (Ind)$CpTaMe_3$.* A solution of 5.00 g of $CpTaMe_3Cl$ [11] (16.8 mmol) in 50 ml of THF was placed into a 250 ml Schlenk flask equipped with a stir bar and a rubber septum. Another solution containing 2.40 g of indenyl sodium (NaInd) (17.4 mmol) in 25 ml of THF was placed in a 50 ml Schlenk flask equipped with a rubber septum. The solution containing the $CpTaMe_3Cl$ was then cooled to −78 °C with a dry ice/acetone bath. The NaInd solution was added via cannula to the cooled solution and the N_2 atmosphere was replaced with argon. This solution was stirred for 2 h at −78 °C, warmed to 0 °C and then stirred an additional 20 min. The solvent was then removed *in vacuo*, taking care not to warm the solution above 0 °C. After the solvent was removed, the remaining brown residue was extracted with 3×50 ml of pentane and then 1×10 ml of toluene. These two solvents were transferred via cannula from Schlenk flasks and then,

after extraction, withdrawn into another Schlenk flask (containing a stir bar) using a cannula fitted with a glass frit. Removal of the solvent *in vacuo* left 4.5 g of Cp(Ind)$TaMe_3Cl$ (11.9 mmol, 71%) pure by ^1H NMR spectrometry. ^1H NMR (C_6D_6, 25 °C): δ 7.03 (dd, $J=6.5$, 3.1, 2H), 6.84 (dd, $J=6.5$, 3.1, 2H), 5.17 (t, $J=3.3$, 1H), 5.02 (d, $J=3.3$, 2H), 4.56 (s, 5H, Cp), 0.366 (s, 6H, Ta–Me_2), −0.055 (s, 3H, Ta–Me). $^{13}C\{^1H\}$ NMR (C_6D_6, 25 °C): δ 126.34(s), 124.76(s), 119.41(s), 112.07(s), 104.19(s), 92.18(s), 31.00(s), 26.36(s). Unfortunately, this compound was extremely temperature sensitive, even in the solid state (white needles started turning into a purple powder within 10 min at room temperature), and was thus used in crude form in the next step.

(2) *Preparation of* $Cp(Ind)TaMe_2^+BF_4^-$. To the flask containing the crude Cp(Ind)$TaMe_3$ was added via cannula a solution of 3.32 g of Ph_3CBF_4 (10.1 mmol) in 30 ml of CH_2Cl_2. This solution was stirred at room temperature for 1 h. The methylene chloride was then removed *in vacuo* and the flask containing the orange residue brought into the dry box. The residue was washed with 3 × 10 ml of toluene, and then the remaining product tritiated with 20 ml of pentane. The light orange powder was dried under a dynamic vacuum for 1 h to leave 2.56 g (5.3 mmol, 53%) of yellow Cp(Ind)$TaMe_2^+BF_4^-$. The compound can be recrystallized to form yellow plates in low yield (10–15%) by Et_2O diffusion onto a saturated acetonitrile solution at −30 °C; m.p. 95–98 °C. ^1H NMR (CD_3CN): δ 7.73 (m, 2H), 7.61 (m, 2H), 6.65 (d, $J=3.2$, 2H), 6.46 (s, 5H, Cp), 6.20 (t, $J=3.2$, 1H), −0.122 (s, 6H, Ta–Me_2). $^{13}C\{^1H\}$ NMR (CD_3CN): δ 132.62(s), 127.80(s), 126.37(s), 113.53(s), 108.43(s), 101.86(s), 56.33(s). MS (FAB): 391 (M^+). HR-MS (FAB): *m/e* calc. for $C_{16}H_{18}BF_4Ta$, 391.0891; found, 391.0889.

$Cp(Ind)Ta(CH_2)_2Ir(CO)_2$ (1b)

(1) *Preparation of* $Cp(Ind)Ta(CH_2)(CH_3)$. To a stirred suspension of 1.54 g of Cp(Ind)$TaMe_2^+BF_4^-$ (3.22 mmol) in 25 ml of THF was added dropwise a solution of 844 mg of $Ph_3P{=}CH_2$ (3.06 mmol) in 20 ml of THF. After stirring for 1 h the solvent was removed *in vacuo*. The tan residue was washed with 25 ml of diethyl ether and the solution suction filtered through a glass frit. The ether was removed *in vacuo* to leave 462 mg (770 μmol, 25%) of a yellow oil of ~65% purity. ^1H NMR (C_6D_6): δ 10.3 (d, 1H, $J=7.3$, CH_2), 9.87 (d, 1H, $J=7.3$, CH_2), 4.91 (s, 5H, Cp), −0.418 (s, 3H, CH_3) (the indenyl resonances could not be confidently assigned). This compound was unstable in solution (decomposition likely occurs via rapid disproportionation to Cp(Ind)Ta(C_2H_4)Me and Cp(Ind)TaMe [11]) and despite repeated attempts could not be purified. Therefore, it was used in crude form in the next step.

(2) *Preparation of* $Cp(Ind)Ta(CH_2)_2Ir(CO)_2$. This compound was prepared by a method analogous to method A for **1a** in which 230 mg of Cp(Ind)Ta(CH_2)(CH_3) (~65% pure, 384 μmol) was reacted with 140 mg of (Ind)$Ir(CO)_2$ (384 μmol) to yield 152 mg of **1b** (62%, 238 μmol) as yellow crystalline needles; m.p. 102–106 °C (dec). ^1H NMR (THF-d_8): δ 7.37 (m, 2H), 7.20 (m, 2H), 5.78 (t, 1H, $J=2.4$), 5.46 (d, 2H, $J=2.4$), 5.12 (d, 2H, $J=12.3$, CH_2), 5.12 (s, 5H, Cp), 4.71 (d, 2H, $J=12.3$, CH_2). $^{13}C\{^1H\}$ NMR (THF-d_8): δ 192.5 (s, CO), 127.3(s), 126.0(s), 115.6(s), 115.1(s), 105.2(s), 100.6(s), 90.7(s). IR (KBr pellet) 2010, 1926, 829, 752 cm^{-1}. UV–Vis (THF) (nm): 351 ($\epsilon=4240$ cm^{-1} M^{-1}), 404 (3660), 454 (774). MS (EI): 638 (M^+), 610 (M^+-CO), 582 (M^+-2CO). HR-MS (EI): *m/e* calc. for $C_{18}H_{16}O_2TaIr$, 638.0260; found, 638.0244.

$Cp_2Ta(CH_2)_2Ir(CO)_2(PEt_3)$ (2)

To a solution of 50 mg of **1a** (85 μmol) in 5 ml of benzene in a 15 ml vial was added 100 μl of PEt_3. The solution was swirled for 5 min. On top of this was layered 10 ml of pentane and the mixture stored at −30 °C to yield 53 mg of white crystalline needles, 88%; m.p. 128–130 °C. ^1H NMR (THF-d_8, −92 °C): δ 5.53 (d, $J=4.7$, 2H, CH_2), 5.19 (s, 10 H, Cp), 4.51 (br, 2H, CH_2), 1.97 (br m, 6H), 1.03 (br m, 9H). $^{13}C\{^1H\}$ NMR (THF-d_8, −98 °C): δ189.48 (d, $J=10.8$, CO), 99.412 (br s, Cp), 98.838 (br s, CH_2), 98.118 (br s, CH_2), 22.676 (br d, $J=34.9$ P–CH_2CH_3), 8.997 (br d, $J=9.1$, P–CH_2CH_3). $^{31}P\{^1H\}$ NMR (THF-d_8, −98 °C): δ −20.1 (s, bound PEt_3), −36.1 (s, free PEt_3). IR (KBr) 2969, 2931, 2874, 1916, 1908, 1862, 825 cm^{-1}. UV–Vis (THF): only absorptions from **1a** were present. *Anal.* Calc. for $C_{20}H_{29}IrO_2PTa$: C, 34.05; H, 4.14. Found: C, 33.63; H, 4.12%.

$Cp_2Ta(CH_2)_2Ir(CO)(dppe)$ (4)

To a solution of 51.2 mg of **1a** (87.1 μmol) in 5 ml of benzene in a 15 ml vial was added 34.7 mg of bis(diphenylphosphino)ethane (87.1 μmol) in 2 ml of benzene with stirring. The yellow solution became orange–red. After 1 h the solvent was removed *in vacuo* to yield a red powder. This was dissolved in 2.5 ml of benzene and filtered through a pad of celite using pressure applied with a pipet bulb. Red crystals (25.7 mg, 31%) were obtained by vapor diffusion of pentane into this solution at room temperature. A second crop (24 mg, 29%) was formed by storing the supernatant at −30 °C for 1 day to give a total yield of 60%; m.p. 215 °C (dec.). ^1H NMR (THF-d_8, −74 °C): δ 7.98 (m, 4H), 7.26 (m, 8H), 7.15 (m, 6H), 5.13 (br s, 4H, μ-CH_2), 4.74 (s, 10H, Cp), 2.52 (br m, 2H, dppe CH_2), 2.15 (br m, 2H, dppe CH_2). $^{13}C\{^1H\}$ NMR (THF-d_8, −74 °C): δ 187.88 (t, $J=23.8$, CO), 141.00 (d, $J=44.7$, *ipso*-Ph), 139.54 (d, $J=34.1$, *ipso*-Ph), 135.38 (m), 131.59

(m), 129.84 (s, *para*-Ph), 128.64 (s, *para*-Ph), 128.52 (m), 128.20 (m), 98.139 (s, Cp), 94.33 (m, μ-CH_2), 94.16 (m, μ-CH_2), 33.34 (m, dppe CH_2). $^{31}P\{^1H\}$ NMR (THF-d_8, −74 °C): δ 44.92. IR (KBr) 3056, 2914, 1867, 1433, 695, 529 cm^{-1}. UV–Vis (C_6H_6): 418 nm (ϵ = 3040 cm^{-1} M^{-1}). *Anal.* Calc. for $C_{39}H_{38}IrOP_2Ta$: C, 48.90; H, 4.00. Found: C, 49.03; H, 4.31%.

$Cp_2Ta(CH_2)_2Ir(CO)_2(CH_3)(I)$ (5a)

To a solution of 100 mg of **1a** (170 μmol) in 10 ml of benzene in a 25 ml round bottom flask equipped with a stir bar and glass stopper was added dropwise 100 μl (1.6 mmol) of methyl iodide. The reaction was stirred for 1 h during which the yellow solution became colorless. The volume of this solution was reduced *in vacuo* to 2 ml. Crystallization was effected by slow vapor diffusion of pentane into the benzene at room temperature to yield 100 mg (137 μmol, 59%) of off-white plates. The remainder of the solvent was removed to give 40 mg (55 μmol, 32%) of additional material of satisfactory (>95%) purity; m.p. 149–151 °C. ^1H NMR (THF-d_8): δ 6.43 (d, 2H, J = 9.9), 5.74 (s, 5H), 5.55 (s, 5H), 5.52 (d, 2H, J = 9.9), −0.178 (s, 3H); (C_6D_6): δ 6.46 (d, 2H, J = 10.1), 5.20 (d, 2H, J = 10.1), 5.08 (s, 5H), 4.49 (s, 5H), −0.393 (s, 3H). $^{13}C\{^1H\}$ NMR (THF-d_8): δ 173.18(s), 105.08(s), 104.10(s), 103.10(s), −19.91(s). IR (THF-d_8): ν(CO) = 2067, 2023 cm^{-1}. UV–Vis (THF): 317 nm (ϵ = 7350 cm^{-1} M^{-1}). *Anal.* Calc. for $C_{15}H_{17}IIrO_2Ta$: C, 24.66; H, 2.33. Found: C, 24.39; H, 2.24%.

$Cp_2Ta(CH_2)_2Ir(CO)(PPh_3)(CH_3)(I)$ (5b)

To a stirred solution of 20 mg of **2** (24 μmol) in 3 ml of THF in a 15 ml vial was added 100 μl of MeI (1.6 mmol) via a syringe. The orange solution became colorless within 5 min. After stirring an additional 5 min the solvent and excess MeI were removed under vacuum. The tan residue was dissolved in 2 ml of benzene and the solution filtered through a pad of celite using pressure applied with a pipet bulb. Crystallization was effected by slow vapor diffusion of pentane into the benzene at room temperature to yield 18 mg (19 μmol, 77%) of off-white blocks of **5b**; m.p. 179–185 °C. ^1H NMR (THF-d_8): δ 7.71 (m, 6H), 7.35 (m, 9H), 6.83 (dd, J(PH) = 4.9, J(HH) = 9.5, 1H, CH_2), 6.27 (dd, J(PH) = 7.7, J(HH) = 9.8, 1H, CH_2), 5.74 (s, 5H, Cp), 5.61 (dd, J(PH) = 5.5, J(HH) = 9.5, 1H, CH_2), 5.40 (s, 5H, Cp), 5.14 (dd, J(PH) = 7.1, J(HH) = 9.8, 1H, CH_2), −0.744 (d, J(PH) = 7.1, 3H, CH_3). $^{13}C\{^1H\}$ NMR (THF-d_8): δ 179.20 (d, J = 3.4, CO), 135.73 (d, J = 8.9, *meta*-Ph), 135.22 (d, J = 47.0, *ipso*-Ph), 130.30 (d, J = 2.0, *para*-Ph), 128.07 (d, J = 9.6, *ortho*-Ph), 111.45 (d, J = 4.3, CH_2), 107.94 (d, J = 37.5, CH_2), 104.07 (s, Cp), 102.43 (s, Cp), −12.14 (d, J = 3.4, CH_3). $^{31}P\{^1H\}$ NMR (THF-d_8): δ −4.53. IR (KBr): 2920, 2000, 1437, 830, 700, 529 cm^{-1}. UV–Vis (THF) (nm): 321 (ϵ = 1900 cm^{-1} M^{-1}), 365 (530). MS (FAB): 963.3 ($M^+ - H$), 949.2 ($MH^+ - CH_3$), 837.2 ($MH^+ - I$), 821.2 ($MH^+ - CH_3I$). HR-MS (FAB): *m/e* calc. for $C_{31}H_{29}IIrOPTa$ ($M^+ - CH_3$), 949.0110; found, 949.0118; calc. for $C_{32}H_{32}IrOPTa$ ($M^+ - I$), 837.1300; found, 837.1291 (the signal corresponding to M^+ was too weak to analyze).

Generation of $Ph_2P(CH_2)_2Ir(CO)_2$ (7a) and $Me_2P(CH_2)_2Ir(CO)_2$ (7b) in solution

A solution of 10.0 mg of **6a** (14 μmol) in 0.5 ml of C_6D_6 was transferred into a Wilmad PS-505 NMR tube. This was connected to a Kontes vacuum adapter via a Cajon joint. The tube was frozen at 77 K and degassed twice. To this frozen solution was added 67.2 torr of CO (28 μmol). The tube was flame sealed and the solution thawed. Spectra were obtained immediately after thawing the solution. ^1H NMR (C_6D_6) δ: 7.54 (m, 7H), 7.32 (m, 5H), 7.00 (m, 13H), 2.09 (dd, J = 8.1, 2.9, 4H). $^{31}P\{^1H\}$ NMR (C_6D_6): δ 37.34(br), 5.96(br). Significant decomposition of **7a** occurred within 1 day at room temperature. Similarly, a solution of 10.0 mg of **6b** (17.5 μmol) in 0.5 ml of C_6D_6 was frozen and degassed. To this mixture was added 84 torr (35 μmol) of CO. The tube was flame sealed and the solution thawed. Spectra were obtained immediately after thawing the solution. ^1H NMR (C_6D_6): δ 7.53 (m, 6H), 7.04 (m, 9H), 0.60 (d, J = 12.1, 6H), 0.46 (d, J = 8.2, 4H). $^{31}P\{^1H\}$ NMR (C_6D_6): δ 33.58, 2.12 (s, br). Significant decomposition of **7b** also occurred within 1 day at room temperature.

$Ph_2P(CH_2)_2Ir(CO)(PPh_3)(CH_3)I$ (8a)

A solution of 105.8 mg of **6a** (152 μmol) in 10 ml of THF was placed in a 25 ml round bottom flask equipped with a stir bar. To this was added dropwise 0.2 ml of CH_3I in 2 ml of THF. The yellow solution became colorless within 1 h. After the solution was stirred for 16 h the solvent was removed under vacuum. The white powder was dissolved in 3 ml of benzene and filtered through a plug of celite. White crystals were obtained by vapor diffusion of pentane onto this solution at 20 °C (97.9 mg, 77%); m.p. 247–249 °C. ^1H NMR (C_6D_6) δ: 7.78 (m, 6H), 7.58 (m, 2H), 7.22 (ddd, J = 11.3, 7.6, 1.4, 2H), 7.05 (m, 6H), 6.91 (m, 9H), 2.83 (ddd, J = 12.2, 6.4, 6.4, 1H), 1.48 (m, 2H), 0.92 (d, J = 5.5, 3H), 0.61 (m, 1H). $^{13}C\{^1H\}$ NMR (C_6D_6) δ: 174.7 (d, J = 5.4, CO), 137.7 (dd, J = 49, 3.7, *ipso*), 135.5 (dd, J = 55.4, 1.8, *ipso*), 135.4 (d, J = 9.5, *meta*), 133.3 (d, J = 47.3, *ipso*), 132.77 (d, J = 2.4, *para*), 132.5 (d, J = 2.5, *para*), 130.7 (d, J = 10.0, *meta*), 130.4 (s, *para*), 130.3 (d, J = 13.0, *ortho*), 129.5 (d, J = 10.5, *ortho*), 129.2 (d, J = 10.6, *ortho*), 128.4 (d, J = 9.7, *meta*), 11.9 (d, J = 2.7, CH_3), −31.1 (dd, J = 41.6, 4.3, CH_2), −39.9

(dd, J=77.0, 46.0, CH_2). $^{31}P\{^1H\}$ NMR (C_6D_6): δ 65.8(s), −0.57(s). IR (KBr): ν(CO) = 1986 cm^{-1}. UV–Vis (THF) (nm): 292 (sh, 5360 cm^{-1} M^{-1}), 328 (sh, 970). HR-MS (FAB): *m/e* calc. for $C_{34}H_{33}OP_2IIr$, 839.0681; found, 839.0658.

$Me_2P(CH_2)_2Ir(CO)(PPh_3)(CH_3)I$ (8b)

A solution of 104.3 mg of **6b** (182 μmol) in 3 ml of THF was placed in a 25 ml round bottom flask equipped with a stir bar. To this was added dropwise 113 μl of CH_3I. The yellow solution became pale immediately. The solution was stirred for 3.5 h and the solvent was then removed under vacuum. The yellow powder was washed with 3×5 ml of pentane, dissolved in 3 ml of benzene and the solution filtered through a plug of celite. Yellow microcrystals (64.0 mg) were obtained by vapor diffusion of pentane onto this solution at room temperature; a second crop (10.3 mg) was obtained by storing the supernatant at −30 °C for 1 day (74.3 mg, 64%); m.p. 195 °C (dec.). ^1H NMR (C_6D_6): δ 7.84 (m, 6H), 7.06 (m, 6H), 6.94 (m, 3H), 1.89 (ddd, J=12.6, 6.3, 6.3, 1H, CH_2), 0.99 (s, 3H, Ir–Me), 0.98 (d, J=18.7, 3H, P–Me), 0.54 (ddd, J=13.3, 6.8, 6.8, 1H, CH_2), 0.38 (ddd, J=12.3, 7.7, 4.6, 1H, CH_2), 0.26 (d, J=12.1, 3H, P–Me), −0.45 (ddd, J=12.3, 7.2, 5.1, 1H, CH_2). $^{13}C\{^1H\}$ NMR (C_6D_6): δ 194.76 (d, J=5.4, CO), 134.74 (d, J=9.4, *ortho*-Ph), 133.00 (d, J=47.2, *ipso*-Ph), 129.72 (d, J=2.2, *para*-Ph), 128.04 (d, J=7.5, *meta*-Ph), 21.16 (dd, J=29.3, 4.0, P–Me), 19.07 (dd, J=33.3, 3.5, P–Me), −11.49, (d, J=3.0, Ir–Me), −27.59 (dd, J=48.8, 3.8, CH_2), −29.28 (dd, J=77.7, 48.7, CH_2). $^{31}P\{^1H\}$ δ 62.4(s), 0.41(s). IR (KBr): ν(CO) = 1981 cm^{-1}. UV–Vis (THF) (nm): 289 (ϵ=3220 cm^{-1} M^{-1}), 326 (570). *Anal.* Calc. for $C_{24}H_{28}IIrOP_2$: C, 40.39; H, 3.96. Found: C, 40.78; H, 4.01%.

$Ph_2P(CH_2)_2Ir(CO)(PPh_3)(CH_2Cl)Cl$ (9)

A solution of 87.9 mg of **6a** (126 μmol) in 4 ml of CH_2Cl_2 was placed in a 25 ml glass bomb, which was then heated in a constant temperature bath at 45 °C for 28 days. The solvent was removed under vacuum, and the residue extracted with 2 ml of benzene. This was filtered through a plug of celite. Off-white cubes were obtained by vapor diffusion of pentane onto this benzene solution, 59.7 mg (61%); m.p. 202–206 °C. ^1H NMR (C_6D_6): δ 7.86 (m, 6H), 7.58 (ddd, J=11.6, 8.1, 1.2, 2H), 7.36 (ddd, J=11.5, 7.7, 1.6, 2H), 7.05 (dt, J=7.6, 2.1, 6H), 6.95 (m, 6H), 6.84 (m, 3H), 4.29 (dd, J=9.9, 8.0, 1H, CH_2Cl), 3.90 (dd, J=8.0, 1.6, 1H, CH_2Cl), 2.32 (ddd, J=12.6, 6.3, 6.3, 1H, CH_2), 2.09 (ddd, J=12.6, 8.2, 4.1, 1H, CH_2), 1.04 (ddd, J=12.6, 8.2, 4.1, 1H, CH_2), 0.26 (m, 1H, CH_2). $^{13}C\{^1H\}$ NMR (C_6D_6): δ 192.9 (d, J(PC) = 6.0, CO), 136.3 (dd, J(PC) = 49.3, 3.8, *ipso* Ph_2P), 134.5 (d, J(PC) = 9.8, J(CH) = 161), 132.8 (dd, J(CP) = 57.2, 2.4, J(CH) = 10, *ipso*), 132.1 (s, *para*), 131.8 (d, J(CP) = 47.3, J(CH) = 8, *ipso*), 130.5 (d, J(CP) = 11.5), 130.3 (d, J(CP) = 10.7), 130.1 (d, J(CP) = 1.6, J(CH) = 161, 7.5), 128.9 (d, J(CP) = 10.6), 128.7 (d, J(CP) = 10.8), 128.4 (d, J(CP) = 8.8), 14.0 (s, J(CH) = 150, CH_2Cl), −23.6 (dd, J(CP) = 41.9, 4.1, J(CH) = 140, CH_2), −32.6 (dd, J=75.5, 44.3, J(CH) = 145, CH_2). $^{31}P\{^1H\}$ NMR (C_6D_6): δ 67.19 (d, J=1.7), 1.28 (d, J=1.7). IR (C_6D_6): ν(CO) = 2018 cm^{-1}. UV–Vis (THF): 250 nm (ϵ = 12 500 cm^{-1} M^{-1}). *Anal.* Calc. for $C_{34}H_{31}Cl_2IrOP_2$: C, 52.30; H, 4.01. Found: C, 51.78; H, 4.07%.

X-ray crystal structure determinations

Crystals of compound **1b**, **2** and **6a** were mounted on glass fibers using polycyanoacrylate cement and coated with the cement to protect them from the atmosphere. The crystal used for data collection was then transferred to a Enraf-Nonius CAD-4 diffractometer and centered in the beam. Automatic peak search and indexing procedures yielded the primitive cell. The final cell parameter and specific data collection parameters for these data sets are given in Table 1.

The raw intensity data were converted to structure factor amplitudes and their e.s.d.s by correction for scan speed, background, and Lorentz and polarization effects. No correction for crystal decomposition was necessary. An empirical correction based on the observed variation in the azimuthal scan data was applied. Removal of systematically absent data left the unique data in the final data set. The structure was solved by Patterson methods and refined via standard least-squares and Fourier techniques.

The quantity minimized by the least-squares program was $\Sigma w(|F_o| - |F_c|)^2$, where w is the weight of a given observation. The p factor, used to reduce the weight of intense reflections, was set to 0.03. The analytical forms of the scattering factor tables for the neutral atoms were used and all scattering factors were corrected for both the real and imaginary components of anomalous dispersion.

Results

Synthesis of Ta–Ir compounds

Reaction of $Cp_2Ta(CH_2)(CH_3)$ with $(Ind)Ir(CO)_2$ (no reaction occurs with $(Ind)Ir(C_2H_4)_2$) resulted in the formation of free indene and $Cp_2Ta(CH_2)_2Ir(CO)_2$ (**1a**) in high isolated yield (Fig. 1). The NMR yield for the same reaction when rapidly stirred in an open vial was 83% indicating that the carbonyl ligands do not dissociate during the reaction. Reaction of $Cp_2Ta(CD_2)(CD_3)$ with $(Ind)Ir(CO)_2$ forms $Cp_2Ta(CD_2)_2Ir(CO)_2$ and indene-d_1, with the deuteron replacing one of the protons in the allylic position of the liberated indene. Both deuterated products have

TABLE 1. Crystal and data collection parameters

	1b	**2**	**6a**
Crystal parameters			
Formula	$C_{18}H_{16}IrO_2Ta$	$C_{20}H_{29}IrO_2PTa$	$C_{33}H_{29}IrOP_2$
Formula weight	637.5	705.6	695.7
Crystal system	monoclinic	monoclinic	triclinic
Space group	$P2_1/n$	$P2_1/n$	$P\bar{1}$
a (Å)	7.050(1)	6.903(2)	9.037(2)
b (Å)	14.314(2)	13.136(3)	12.423(3)
c (Å)	15.659(2)	22.875(3)	13.946(3)
α (°)	90.0	90.0	70.896(16)
β (°)	93.034(10)	98.56(2)	79.450(17)
γ (°)	90.9	90.0	72.270(18)
V (Å^3)	1578.0(7)	2051.1(17)	1403.1(6)
Z	4	4	2
Crystal dimensions (mm)	0.12×0.25×0.40	0.20×0.25×0.35	0.15×0.20×0.35
Color	yellow	red	yellow
D_{calc} (g cm^{-3})	2.68	2.28	1.65
μ_{calc} (cm^{-1})	152.5	118.2	48.7
Data collection			
Temperature (K)	155	188	172
Diffractometer		Enraf-Nonius CAD-4	
Monochromator		highly-oriented graphite (2θ=12.2)	
Radiation		Mo Kα (λ=0.70926 Å)	
2θ Range (°)	3–45	3–45	3–45
Scan type	θ–2θ	θ–2θ	θ–2θ
Scan speed (°/min)	constant, 6.70	constant, 6.70	constant, 6.70
Data collected	$+h, +k, \pm l$	$+h, +k, \pm l$	$+h, \pm k, \pm l$
Background		measured over 0.25*($\Delta\theta$) added to each end of the scan	
Crystal decay	no	no	no
No. reflections collected	2166	3078	3658
No. independent reflections	2061	2677	3658
No. observed reflections	1818 ($F^2>3\sigma F^2$)	2317 ($F^2>3\sigma F^2$)	3285 ($F^2>3\sigma F^2$)
Absorption correction	empirical	empirical	empirical
Min./max. transmission	0.455/0.995	0.531/0.922	0.774/0.999
Solution and refinement			
No. parameters refined	99	117	164
$R(F)$ (%)	2.7	3.3	3.1
$R_w(F)$ (%)	3.4	4.3	4.1
R_{all} (%)	3.3	4.3	3.6
Goodness of fit	1.62	2.03	1.95
p-Factor	0.03	0.03	0.03

been identified by ^{1}H NMR spectrometry. Neither $CpIr(CO)_2$ nor $Cp^*Ir(CO)_2$ reacts with $Cp_2Ta(CH_2)(CH_3)$.

An alternative, high-yield method of synthesizing **1a** was developed by treating $Cp_2Ta(CH_2)(CH_3)$ with $IrCl(CO)_2(NH_2tol)$ in the presence of the base $KN(TMS)_2$. In the absence of added base, the yield of this reaction is only 18% on a 10 μmol scale and essentially no **1a** can be recovered when the reaction is run on a larger scale.

Compound **1a** is air stable. Unlike most early transition metal organometallic complexes, the material is also relatively water stable, decomposing only upon heating to 100 °C for 3 h in the presence of 5 equiv. of water in toluene-d_8. The IR spectrum of **1a** reveals two absorbances at 1946 and 2008 cm^{-1}. The ^{1}H NMR spectrum shows equivalent Cp groups at 4.44 ppm and equivalent CH_2 groups at 5.28 ppm in C_6D_6. The $^{13}C\{^1H\}$ spectrum of **1a** exhibits singlets for the methylene groups at 108.9 ppm and the Cp ligands at 100.0 ppm.

$Cp(Ind)Ta(CH_2)_2Ir(CO)_2$ (**1b**) is obtained in moderate yield from the reaction of $Cp(Ind)Ta(CH_2)(CH_3)$ with $(Ind)Ir(CO)_2$. Compound **1b** has spectroscopic properties similar to those of **1a**. The CO stretching

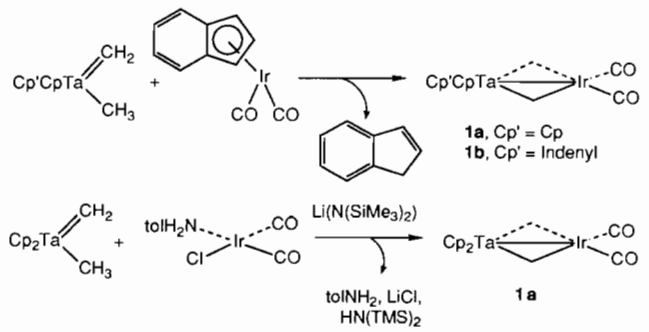

Fig. 1. Synthesis of $Cp_2Ta(CH_2)_2Ir(CO)_2$.

absorptions appear at 2010 and 1926 cm^{-1} in the IR spectrum. The bridging methylene hydrogens exhibit an AA'BB' pattern with $J_{AB}=12.3$ Hz and appear at 5.12 and 4.71 ppm in THF-d_8. The indenyl resonances in the ^1H NMR and ^{13}C NMR spectra appear at regions typical for η^5-bound indenyl groups [16]. Finally, the UV–Vis spectra of **1a** and **1b** are nearly identical with peaks at 354, 404 and 456 nm and 351, 404 and 454 nm, respectively. Unlike **1a**, compound **1b** is unstable above 60 °C in solution, perhaps due to reactions that occur via indenyl ring slip at the tantalum center.

Crystals of **1b** suitable for an X-ray diffraction study were grown by slow vapor diffusion of pentane into toluene (Fig. 2 and Tables 2 and 3). This revealed that the $Ta(CH_2)_2Ir$ bimetallacycle is completely planar. The geometry about the Ta center is pseudo-tetrahedral, with the indenyl ligand bound in an η^5-fashion. The iridium center geometry is square planar. The Ta–CH_2–Ir angles are 83°, and the Ta–Ir bond distance (2.858(1) Å) places the metals within estimated van der Waals distances of each other. Because of this (and other evidence; see below) we believe this complex contains a metal–metal bond. The Ta–CH_2 (2.126(8) Å) and Ir–CH_2 (2.181(8) Å) bonds are nearly identical in length. The Ind–Ta–Ir angle (109.9°) is smaller than the Cp–Ta–Ir angle (117.3°).

Reaction of 1a with PR_3

Triethylphosphine reacts with **1a** to give the off-white compound $Cp_2Ta(CH_2)_2Ir(CO)_2(PEt_3)$ (**2**) in high yield (Fig. 3). The compound shows two CO stretches in the IR spectrum at 1912 (the band is actually split into absorbances at 1908 and 1916 cm^{-1}; this is likely a solid state effect) and 1862 cm^{-1}. Although quite stable as a solid, the complex loses PEt_3 upon dissolution in THF-d_8, as evidenced by sharp signals for **1a** and PEt_3 in a 1:1 ratio in the ^1H NMR spectrum at room temperature. At −95 °C the spectrum changes, now showing 1 Cp and 2 broad CH_2 resonances due to **2**.

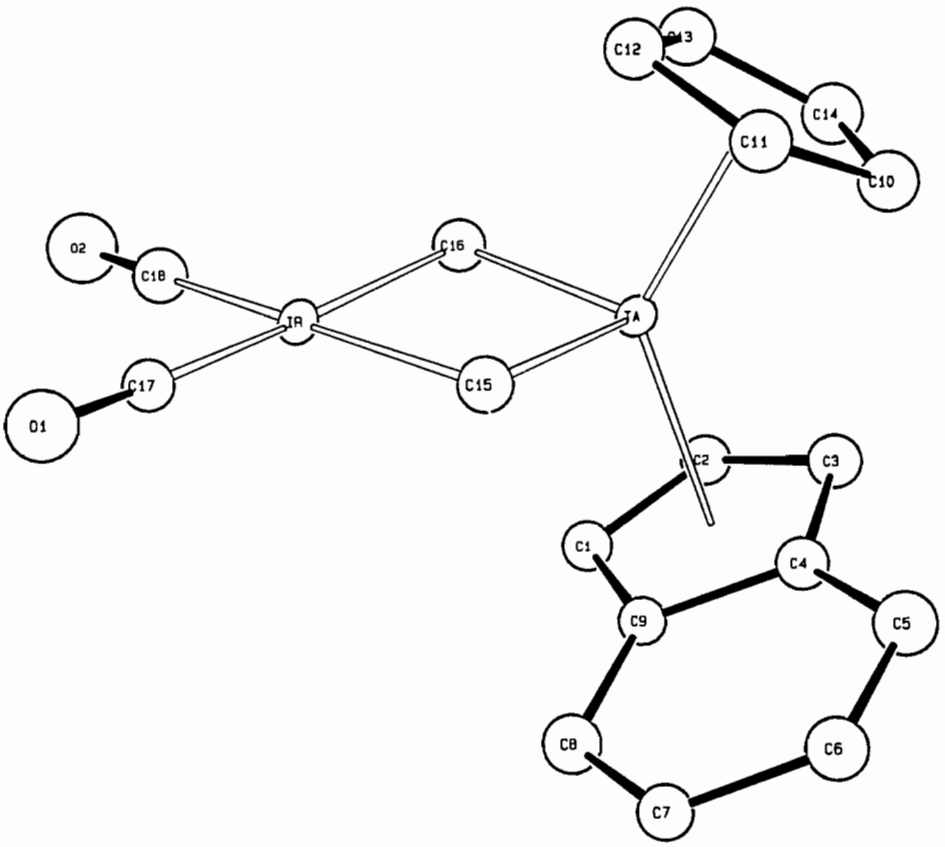

Fig. 2. ORTEP diagram of (indenyl)CpTa$(CH_2)_2Ir(CO)_2$ (**1b**).

TABLE 2. Selected bond lengths and angles for (indenyl)CpTa$(CH_2)_2$Ir$(CO)_2$ (**1b**)

Bond lengths (Å)		Bond angles (°)	
Ta–Ir	2.858(1)	C15–Ir–C16	95.4(3)
Ta–C15	2.126(8)	C17–Ir–C18	97.9(3)
Ir–C15	2.181(8)	Ir–C15–Ta	83.1(3)
Ta–Cp	2.098	C15–Ta–C16	98.0(3)
Ta–Ind	2.151	Cp–Ta–Ind	132.8
Ta–C3	2.375(8)	C16–Ir–C18	83.4(3)
Ta–C9	2.594(8)	Ind–Ta–Ir	109.9
Ta–C4	2.491(8)	Cp–Ta–Ir	117.3
Ir–C18	1.842(8)		
C18–O2	1.175(9)		
Ta–C2	2.410(8)		
Ta–C1	2.465(8)		

TABLE 3. Table of positional parameters ($\times 10^3$) for (indenyl)CpTa$(CH_2)_2$Ir$(CO)_2$ (**1b**) and their e.s.d.s

Atom	*x*	*y*	*z*
Ir	170.22(5)	114.82(3)	376.61(2)
Ta	80.61(5)	−38.68(3)	264.98(2)
O1	−65.2(9)	275.8(5)	431.4(5)
O2	538(1)	166.9(6)	472.3(5)
C1	263(1)	53.6(7)	164.6(6)
C2	300(1)	−44.2(7)	152.2(6)
C3	129(1)	−87.5(7)	122.8(7)
C4	−10(1)	−16.0(7)	110.5(6)
C5	−207(1)	−18.2(7)	78.2(7)
C6	−300(1)	65.0(7)	69.2(7)
C7	−214(1)	152.7(7)	89.9(6)
C8	−30(1)	157.4(7)	123.1(7)
C9	76(1)	72.0(7)	133.8(6)
C10	−118(1)	−177.6(7)	250.4(7)
C11	−189(1)	−120.4(7)	316.1(7)
C12	−55(1)	−115.0(7)	385.3(7)
C13	105(1)	−169.8(7)	362.9(7)
C14	70(1)	−207.4(7)	280.6(7)
C15	−90(1)	74.0(7)	304.7(6)
C16	332(1)	−6.8(7)	341.8(7)
C17	26(1)	213.4(7)	409.0(6)
C18	393(1)	147.7(7)	435.5(7)
Cp1	151.5	−4.4	136.7
Cp2	−37.3	−158.0	319.0

We assume that this is due to a shift in equilibrium toward **2**, but that reversible PEt_3 dissociation is still proceeding at this temperature.

A single crystal X-ray diffraction study was carried out on **2** (Fig. 4 and Tables 4 and 5). The geometry about the iridium center lies midway between a square-based pyramid (with the CH_2 group *cis* to the phosphine as the apical ligand) and a trigonal bipyramid (with the PEt_3 ligand and the CH_2 group *trans* to it as the axial ligands). The bimetallacycle is once again completely planar with bond distances and angles very similar to that of **1b** and a Ta–Ir bond distance only slightly longer at 2.881(1) Å. The Ir–CH_2 bond lengths for the groups *cis* and *trans* to the PEt_3 ligand are substantially different, 2.219(8) and 2.161(8) Å, respectively. Again, the geometry about the Ta center is pseudo-tetrahedral.

In contrast to its behavior with PEt_3, reaction of **1a** with PPh_3 leads to the formation of the substitution product $Cp_2Ta(CH_2)_2Ir(CO)(PPh_3)$ (**3**), in which the iridium center is four-coordinate (Fig. 3). Consistent with this formulation only a single CO stretch at 1937 cm^{-1} (KBr) is present in the IR spectrum. The Cp groups are equivalent and the CH_2 groups inequivalent by both ^1H and $^{13}C\{^1H\}$ NMR spectrometry. The elemental analysis of **3** is also consistent with the replacement of a CO ligand by PPh_3.

Reaction of **1a** with bis(diphenylphosphino)-ethane (dppe) leads to the formation of $Cp_2Ta(CH_2)_2Ir(CO)(dppe)$ (**4**) (Fig. 3), which is highly fluxional at room temperature. At all observed temperatures, the $^{31}P\{^1H\}$ NMR spectrum is a singlet, but at −74 °C the line is very sharp while at 55 °C the line is >200 Hz wide. In the ^1H NMR spectrum at 55 °C, the dppe ethylene bridge resonances are equivalent with coupling to magnetically inequivalent P nuclei. As the sample is cooled, the P-bridge resonance becomes a singlet and then broadens out into two complex multiplets at −50 °C. The Cp groups are equivalent by ^1H and $^{13}C\{^1H\}$ NMR at all temperatures. However, whereas the resonance for the metal-bridging CH_2 groups is a slightly broad singlet in the ^1H NMR at −74 °C, in the $^{13}C\{^1H\}$ NMR spectrum the resonance associated with these methylenes is a set of eight lines, consistent with the presence of two inequivalent groups. At −70 °C, the $^{13}C\{^1H\}$ NMR spectrum reveals the presence of a CO ligand coupled to two equivalent phosphorus nuclei. The IR spectrum of **4** reveals one CO stretching absorption at 1867 cm^{-1}, 70 cm^{-1} lower in energy than the ν(CO) for **3**.

Oxidative addition of MeI to 1a

Compound **1a** reacts at room temperature with CH_3I to form the oxidative addition product $Cp_2Ta(CH_2)_2Ir(CO)_2(CH_3)(I)$ (**5a**) in high yield (Fig. 3). Compound **5a** is nearly colorless (only a single band is seen in the UV–Vis spectrum at 316 nm, which tails off just into the visible region), suggesting a d^6-octahedral geometry. Two CO stretches are present in the IR spectrum at 2023 and 2067 cm^{-1}, approximately 70 cm^{-1} higher in energy than those in **1a**. The Cp ligands are inequivalent by ^1H NMR spectrometry, and the CH_2 groups appear as an AA'BB' pattern with $J_{AB}=9.9$ Hz. However, only one type of CH_2 group is observed in the $^{13}C\{^1H\}$ spectrum. These data indicate that CH_3I adds to the iridium center in a *trans* fashion.

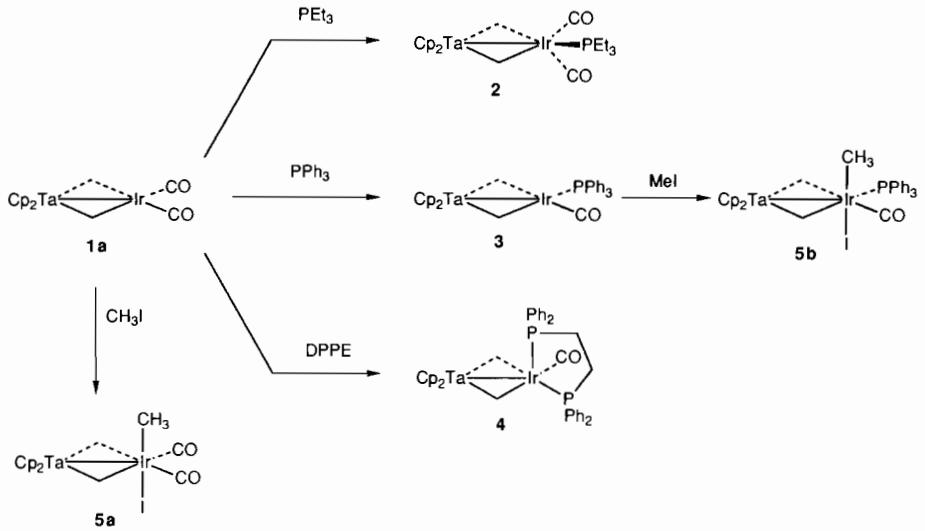

Fig. 3. Reactions of $Cp_2Ta(CH_2)_2Ir(CO)_2$.

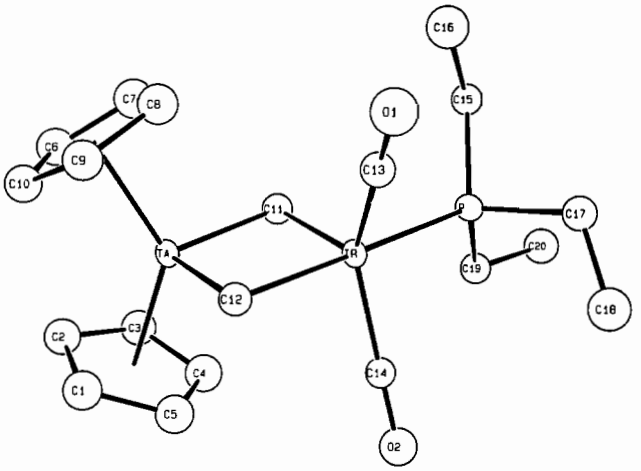

Fig. 4. ORTEP diagram of $Cp_2Ta(CH_2)_2Ir(CO)_2(PEt_3)$ (2).

TABLE 4. Selected bond lengths and angles for $Cp_2Ta(CH_2)_2Ir(CO)_2(PEt_3)$ (2)

Bond lengths (Å)		Bond angles (°)	
Ta–Ir	2.881(1)	C11–Ir–C12	95.1(3)
Ta–C11	2.126(8)	Ir–C12–Ta	83.7(3)
Ta–C12	2.156(8)	Ir–C11–Ta	83.1(3)
Ta–Cp1	2.112	C11–Ta–C12	98.0(3)
Ir–C11	2.219(8)	Cp1–Ta–Cp2	131.8
Ir–C12	2.161(8)	C12–Ir–P	178.9(2)
Ir–C13	1.832(8)	C13–Ir–C14	134.4(3)
Ir–P	2.308(2)	C11–Ir–C13	117.7(3)
P–C15	1.843(8)	C12–Ir–C13	85.1(3)
C13–O1	1.192(10)	P–Ir–C13	93.9(3)

Compound **3** also reacts with MeI to form the oxidative addition product $Cp_2Ta(CH_2)_2Ir(CO)(PPh_3)(CH_3)(I)$ (**5b**) in good yield (Fig. 3). The spectroscopic properties of **5b** are similar to those of **5a**. The rate of oxidative addition of MeI to **3** was measured in THF at −5 °C and found to be first order in both reagents. The second order rate constant for addition is $7.61 \pm 0.43\ M^{-1}\ s^{-1}$.

TABLE 5. Table of positional parameters for $Cp_2Ta(CH_2)_2Ir(CO)_2(PEt_3)$ (2) ($\times 10^3$) and their e.s.d.s

Atom	*x*	*y*	*z*
Ir	−15.14(6)	225.31(3)	99.40(2)
Ta	−0.98(6)	99.49(3)	203.12(2)
P	−265.3(4)	263.9(2)	24.0(1)
O1	48(1)	443.4(7)	140.1(4)
O2	190(1)	90.5(6)	20.6(4)
C1	235(2)	−37(1)	220.7(6)
C2	55(2)	−73.2(9)	237.5(6)
C3	−89(2)	−77.7(9)	184.3(6)
C4	4(2)	−48(1)	136.2(6)
C5	203(2)	−23(1)	157.6(6)
C6	−150(2)	97.1(9)	293.0(6)
C7	−233(2)	181(1)	259.3(6)
C8	−84(2)	252(1)	252.7(6)
C9	98(2)	211.9(9)	286.0(6)
C10	52(2)	119.1(9)	308.8(5)
C11	−239(2)	133.8(9)	135.9(5)
C12	218(2)	192.0(9)	170.8(5)
C13	19(2)	357.8(9)	123.9(5)
C14	108(2)	140.6(8)	51.1(5)
C15	−492(2)	319.0(9)	44.1(5)
C16	−457(2)	404(1)	89.2(6)
C17	−201(2)	356.8(9)	−29.1(5)
C18	−31(2)	323(1)	−61.3(6)
C19	−353(2)	151.9(9)	−21.2(5)
C20	−515(2)	170(1)	−74.1(6)

Reactivity of P–Ir complexes $Ph_2P(CH_2)_2Ir(CO)(PPh_3)$ (6a) and $Me_2P(CH_2)_2Ir(CO)(PPh_3)$ (6b)

Compounds **6a** and **6b** were prepared in high yield by treatment of the ylide anions $Ph_2P(CH_2)_2Li$ and $Me_2P(CH_2)_2Li$ with Vaska's complex, $(PPh_3)_2Ir(CO)Cl$

(Fig. 5). Both **6a** and **6b** show some spectroscopic similarities to the heterodinuclear compound $Cp_2Ta(CH_2)_2Ir(CO)(PPh_3)$ (**3**), mostly notably the CO stretching vibrations in C_6D_6 (**3**: 1934; **6a**: 1934; **6b**: 1929 cm^{-1}). However, the μ-CH_2 groups appear at very different chemical shifts in the ^1H NMR (**3**: 5.42, 4.32; **6a**: 1.47, 0.37; **6b**: 1.20, −0.84 ppm) and in the ^{13}C NMR (**3**: 116.7, 109.6; **6a**: unobservable at any temperature; **6b**: −5.00, −16.73 ppm) spectra.

The results of a single crystal X-ray diffraction study of **6a** are presented in Fig. 6 and Tables 6 and 7. The ylide phosphorus atom has a slightly distorted tetrahedral geometry and the iridium center is nearly square planar. However, the most striking feature of this structure is that the four-membered metallacycle is not planar as it is in both of the Ta–Ir structures described above. We therefore represent **6a** as a zwitterion (Fig. 5), a consequence of the lack of significant direct P–Ir bonding. The dihedral angle between the two planes of the four-membered ring is 144.08 ± 0.42°. The bond angle about the bridging methylenes is 88° and the bond angle about the iridium center is 75.21(20)°. The Ir–PPh_3 bond distance is 2.261(1) Å, nearly 0.5 Å shorter than the iridium phosphorus ylide non-bonding distance of 2.746(1) Å. The Ir–CH_2 bond lengths do not differ substantially for the group *cis* (2.175(5) Å) and *trans* (2.162(5) Å) to the PPh_3 ligand. The average P–CH_2 bond length is 1.76 Å. This is shorter than a P–C single bond (typically *c.* 1.87 Å [17]) and can be considered the upper limit of a double bond [18].

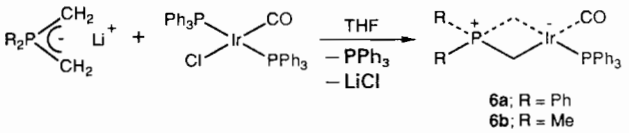

Fig. 5. Synthesis of $Ph_2P(CH_2)_2Ir(CO)(PPh_3)$ and $Me_2P(CH_2)_2Ir(CO)(PPh_3)$.

Compound **6a** shows fluxional behavior in its $^{13}C\{^1H\}$ and $^{31}P\{^1H\}$ NMR spectra. At room temperature a sharp ^{31}P resonance at 32.1 ppm is observed for the ylide phosphorus atom of **6a** and a broad resonance at 28.6 ppm is observed for the PPh_3 ligand. Cooling the solution to −98 °C results in sharpening of the broad resonance but no change in the chemical shift is seen. A slight change in the chemical shift (1.1 ppm downfield) is observed for the ylide phosphorus atom. Similar behavior is seen for compound **6b**.

Addition of 1 equiv. of PPh_3 to a solution of **6a** resulted in a $^{31}P\{^1H\}$ NMR spectrum in which the broad resonance was shifted to 11.73 ppm, halfway between the shift of free PPh_3 and PPh_3 bound to **6a**. A resonance was not observed for free PPh_3. Cooling this solution to −109 °C caused the broad peak to split into two separate broadened resonances, one of which can be attributed to free PPh_3. Analogous results were seen upon addition of other phosphines ($PTol_3$ or PMe_3) to solutions of **6a**. Although a full VT study was not performed for the addition of PPh_3 to **6b**, similar behavior is apparent in the room temperature $^{31}P\{^1H\}$ spectrum. However, even in the presence of trace amounts of free PPh_3 (<0.1 equiv.) the resonances for

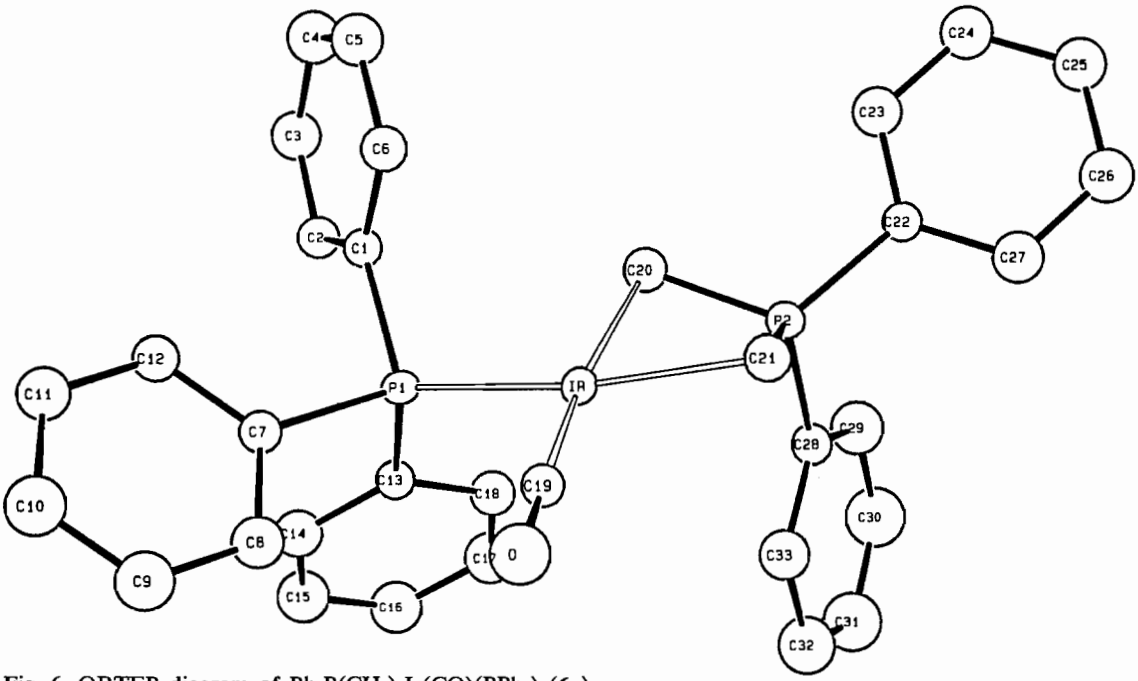

Fig. 6. ORTEP diagram of $Ph_2P(CH_2)_2Ir(CO)(PPh_3)$ (**6a**).

TABLE 6. Selected bond lengths and angles for $Ph_2P(CH_2)_2Ir(CO)(PPh_3)$ (**6a**)

Bond lengths (Å)		Bond angles (°)	
P1–Ir	2.261(1)	C20–Ir–C21	75.21(20)
P2–Ir	2.746(1)	Ir–C20–P2	87.89(22)
P2–C20	1.759(5)	Ir–C21–P2	88.13(22)
P2–C21	1.765(5)	C20–P2–C21	97.4(3)
Ir–C20	2.175(5)	C22–P2–C28	105.30(24)
Ir–C21	2.162(5)	C19–Ir–P1	97.55(16)
Ir–C19	1.800(5)	C20–Ir–P1	92.01(14)
P1–C1	1.828(5)	C19–Ir–C21	95.23(21)
P2–C22	1.824(5)		
P2–C28	1.797(5)		
C19–O	1.181(6)		

TABLE 7. Table of positional parameters for $Ph_2P(CH_2)_2Ir(CO)(PPh_3)$ (**6a**) ($\times 10^3$) and their e.s.d.s

Atom	*x*	*y*	*z*
Ir	228.43(3)	141.30(2)	361.83(2)
P1	149.7(2)	279.9(1)	215.7(1)
P2	134.3(2)	151.0(2)	558.3(1)
O	512.8(6)	−4.3(5)	272.9(4)
C1	−61.7(8)	319.9(5)	212.1(5)
C2	−151.1(8)	435.7(6)	176.6(5)
C3	−311.8(9)	460.3(7)	177.9(6)
C4	−383(1)	367.0(7)	212.9(6)
C5	−295.2(9)	251.1(7)	247.3(6)
C6	−133.3(8)	228.1(6)	247.9(5)
C7	223.8(8)	250.9(6)	91.8(5)
C8	384.2(9)	209.1(6)	71.3(6)
C9	443(1)	181.6(7)	−20.8(6)
C10	343(1)	196.3(7)	−91.9(6)
C11	182.2(9)	240.4(6)	−71.3(6)
C12	121.8(8)	266.3(6)	20.8(5)
C13	192.0(8)	422.5(6)	194.9(5)
C14	226.8(9)	492.9(6)	98.3(6)
C15	260(1)	599.7(7)	87.5(6)
C16	262(1)	634.2(7)	170.4(6)
C17	229(1)	562.9(7)	268.8(6)
C18	193.7(9)	455.6(6)	280.9(6)
C19	400.2(8)	55.0(6)	306.7(5)
C20	25.9(8)	219.2(6)	451.6(5)
C21	257.4(8)	30.8(6)	516.9(5)
C22	23.1(8)	114.1(6)	682.1(5)
C23	−133.0(9)	124.6(6)	686.6(6)
C24	−215.6(9)	83.3(7)	781.2(6)
C25	−139.6(9)	31.3(7)	868.5(6)
C26	19(1)	18.6(7)	863.3(6)
C27	102.3(9)	60.9(6)	770.2(6)
C28	245.5(8)	244.0(6)	568.4(5)
C29	179(1)	321.6(7)	627.8(6)
C30	264(1)	396.4(8)	636.6(7)
C31	416(1)	387.8(8)	587.1(7)
C32	482(1)	311.8(7)	527.4(7)
C33	395.3(9)	239.4(6)	517.6(6)

bound and free PPh_3 disappear into the baseline (only the ylide phosphorus is observable).

Reaction of carbon monoxide with **6a** or **6b** resulted in the formation of the unstable dicarbonyl compounds $R_2P(CH_2)_2Ir(CO)_2$ **7a** and **7b**, respectively (Fig. 7). A single CH_2 resonance and equivalent Ph and Me resonances in the ^1H NMR spectrum are consistent with the proposed structure. However, both compounds were 50% decomposed within 1 day.

Compounds **6a** and **6b** react with MeI to form the oxidative addition products **8a** and **8b** (Fig. 7). Unlike their parent compounds, these compounds do not exhibit temperature dependent behavior. The $^{31}P\{^1H\}$ NMR spectrum of **8a** reveals two sharp singlets at 65.8 and −0.57 ppm. The CO stretching absorption in the IR spectrum appears at 1986 cm^{-1}. The rates of oxidative addition of MeI to both **6a** and **6b** were measured in THF at −5 °C and found to be first order in each reagent. The second order rate constant for the addition to **6a** was 7.55 ± 0.30 M^{-1} s^{-1} and to **6b** 17.9 ± 1.4 M^{-1} s^{-1}.

Compound **6a** also reacts slowly with CH_2Cl_2 to give the oxidative addition product **9** (Fig. 7) [19]. However, the reaction requires several weeks at 45 °C in neat CH_2Cl_2 to go to completion. Four different signals are present in the ^1H NMR spectrum for the hydrogens on the μ-CH_2 groups, verifying the chiral environment at the iridium center. The $^{13}C\{^1H\}$ NMR spectrum reveals two different μ-CH_2 groups, one with a $J(CP)$ of 4.1 Hz and one of 75 Hz; the carbonyl signal appears at 192.9, with $J(CP) = 6.0$ Hz. The CO stretch in the IR spectrum is observed at 2016 cm^{-1}.

^{13}C–^1H coupling constants

In order to determine whether the bond angles and bond distances of complexes such as **1b, 2** and **6a** can

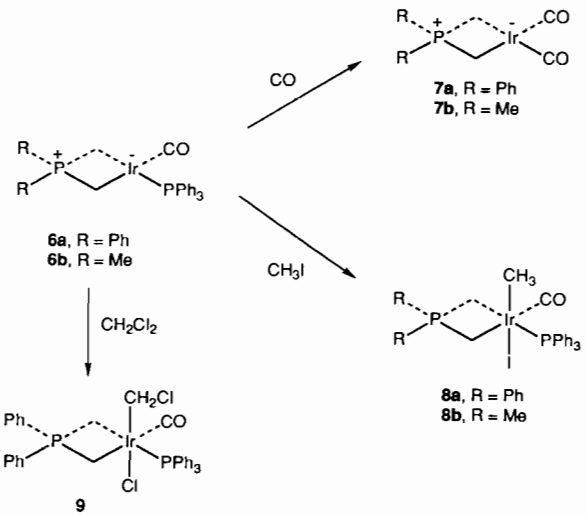

Fig. 7. Reactions of $Ph_2P(CH_2)_2Ir(CO)(PPh_3)$ and $Me_2P(CH_2)_2Ir(CO)(PPh_3)$.

be correlated with the hybridization at the carbon centers as determined by ^{13}C NMR, $J(CH)$ values for several of the compounds described here were measured. The observed $J(CH)$ at the μ-CH_2 carbon in **1a** is 136 Hz; upon oxidative addition of MeI $J(CH)$ increases slightly to 139 Hz. Oxidative addition of Et_3SiH to **1a** increases $J(CH)$ to 136 and 139 [20]. The coupling constant for the C–H groups on the cyclopentadienyl ring of **1a** is 178 Hz (coupling of the Cp carbon atoms to the μ-CH_2 protons was also evident, with $J(CH) = 6.7$ Hz). Typically, $J(CH)$ at the μ-CH_2 groups of the corresponding P–Ir complexes were slightly, but uniformly, higher: 138 and 142 Hz for **6a**. The CH_2Cl_2 oxidative addition product **9** exhibits ^{13}C–^1H coupling constants of 140 (for the CH_2 *cis* to PPh_3)*, 145 (for the CH_2 *trans* to PPh_3)* and 150 (for the CH_2Cl) Hz. The $J(CH)$ for the aromatic ring carbons of the PPh_3 and PPh_2 groups all showed typical sp^2 values of 161 ± 1 Hz.

Discussion

Synthetic studies

Based on our earlier studies [21] and the work of Stone and co-workers [22], we believe that the reaction of $Cp_2Ta(CH_2)(CH_3)$ with $(Ind)Ir(CO)_2$ leads initially to intermediate **10** (Fig. 8) followed by intramolecular oxidative addition of the Ta–methyl C–H bond to give the η^1-indenyl complex **11**. We had expected **11** to lose two COs, leading to $Cp_2Ta(CH_2)_2Ir(Ind)H$ (**12**), but instead **1a** was formed by reductive elimination of indene. Consistent with this mechanistic hypothesis, the use of $Cp_2Ta(CD_2)(CD_3)$ in the reaction results in formation of indene with one deuterium in the allylic position.

Several pieces of evidence support the proposition that the first step in the mechanism involves binding of the $Ta{=}CH_2$ fragment to the iridium center, with subsequent 'slippage' of the indenyl ring to an η^3-mode of binding. First, the $Ta{=}CH_2$ fragment has been shown to bind in an η^2-manner in the complex $Cp_2Ta(CH_2)(CH_3)Pt(PMe_3)_2$ formed from the reaction of $Cp_2Ta(CH_2)(CH_3)$ with $(PMe_3)_2Pt(C_2H_4)$ [21]. Second, the bulky analogue $CpCp^*Ta(CH_2)(CH_3)$ does not react with $(Ind)Ir(CO)_2$. Third, indenyl rings in other systems are well-known to undergo η^5-to η^3-isomerization upon coordination of another ligand [23]. Finally, neither $CpIr(CO)_2$ nor $Cp^*Ir(CO)_2$ reacts with $Cp_2Ta(CH_2)(CH_3)$.

An alternative method for preparing **1a** involves treatment of $Cp_2Ta(CH_2)(CH_3)$ with the base

*All four of the μ-CH_2 protons are chemically inequivalent, but the two C–H coupling constants at the same carbon have the same values.

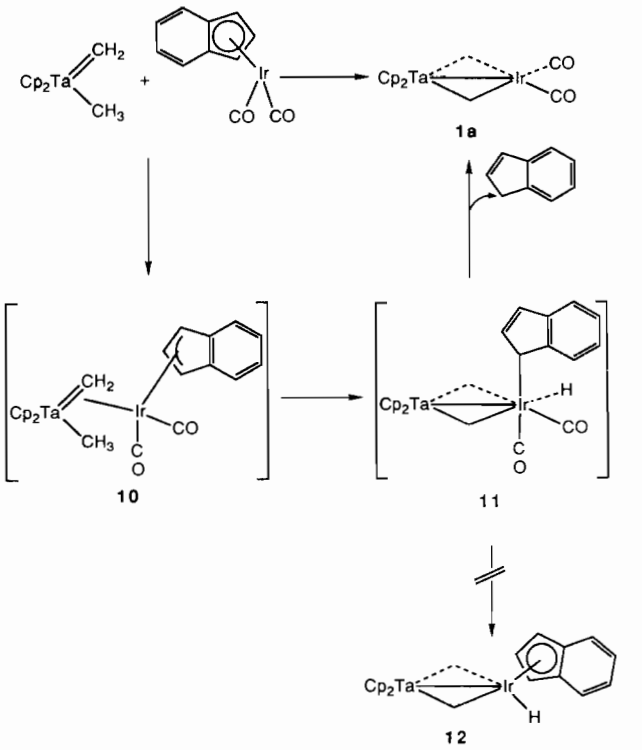

Fig. 8. Proposed mechanism for the synthesis of $Cp_2Ta(CH_2)_2Ir(CO)_2$ from the reaction of $Cp_2Ta(CH_2)(CH_3)$ with $(Indenyl)Ir(CO)_2$.

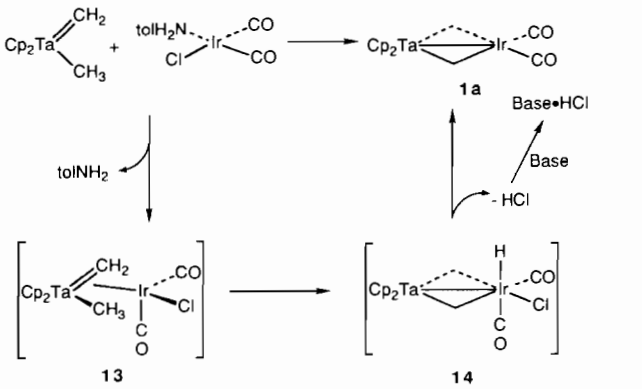

Fig. 9. Proposed mechanism for the synthesis of $Cp_2Ta(CH_2)_2Ir(CO)_2$ from the base-promoted reaction of $Cp_2Ta(CH_2)(CH_3)$ with $Ir(CO)_2Cl(NH_2tol)$.

$KN(TMS)_2$ and $IrCl(CO)_2(NH_2tol)$. We believe this reaction does not involve initial deprotonation of the $Ta{-}CH_3$ group, nor deprotonation of the Ir(III) hydrido chloride intermediate (**14**). Instead, we suggest that the base functions only by absorbing HCl after it is reductively eliminated from **14** (Fig. 9). We draw this conclusion because there is no reaction between $Cp_2Ta(CH_2)(CH_3)$ and $KN(TMS)_2$ or even between $Cp_2Ta(CH_2)(CH_3)$ and the stronger base n-BuLi. This has been shown further to proceed not by deprotonation, but (using the hindered base 2,6-di-tert-butyl pyridine)

by absorption of free HCl [24]. The reaction of $Cp_2Ta(CH_2)(CH_3)$ with $IrCl(CO)_2(NH_2tol)$ in the absence of base proceeds in low yield and only when the reaction is run on a small scale. Here the HCl is likely absorbed by free PPh_3 or basic sites on the glassware. This base-promoted methodology has been applied more recently to the synthesis of a range of other Ta–Rh and Ta–Ir compounds [24].

Comparative Ta, P chemistry

Structural studies

The bimetallacycle is completely planar in **1b** and **2**. The Ta–CH_2 bond length (2.132(8) Å) is intermediate between average bond lengths for Ta–CH_2R (2.26 Å) and Ta=CHR (2.02 Å) [25]. There is evidence that a Ta–Ir metal–metal bond is present in these molecules. The Ta and Ir atoms of both molecules are within single bond distance of each other, and in addition the Ta–CH_2–Ir bond angles are more acute than would be expected for a cyclobutane-based structure. The slightly larger bond angles and bond distances for **2** (relative to **1b**) are likely due to steric interactions between the ligands on the iridium center and the Cp ligands on the tantalum.

The lack of planarity of metallacycle **6a** shows that there are clear structural effects of changing Ta to P. It seems likely that this is a result of the lack of interaction between the iridium center and the ylide phosphorus atom, which are well beyond van der Waals distances. The P–CH_2–Ir bond angles are extended 5° relative to **1b** and **2**.

Bonding in Ta–Ir and P–Ir complexes

Five resonance structures for the Ta–Ir and P–Ir complexes can be envisaged (Fig. 10): structure A, in which no bond exists between the two centers and the molecule is formally zwitterionic; structure B, in which the iridium center has donated an electron pair to the Ta(P); structures C and D, which have 1 Ir–CH_2 σ bond and 1 Ir–CH_2 π bond, and there exists a Ta(P)=CH_2 double bond; and structure E, in which the Ta(P)$(CH_2)_2$ is coordinated like an edge-bound allyl group to the iridium center (this can perhaps be thought of as a resonance hybrid of structures C and D). The crystal structure data imply a predominance of resonance structure A for **6a**, whereas for **1b** and **2**, no single dominant structure can be assigned.

A proposed molecular orbital (MO) diagram for the Ta–Ir compound is shown in Fig. 11 (for the ylide P–Ir complexes, the MO diagram should be the same as that for a typical square-planar d^8 iridium center [26]). On the left side of the diagram are the frontier orbitals for a d^1 Cp_2Ta fragment and on the right side, the orbitals for a d^7 $Ir(CO)_2$ fragment [26]. The bridging methylenes were chosen to be formally $(CH_2)^{2-}$. They combine with the b_2 and $2a_1$ orbitals on tantalum and the b_2 and $3a_1$ orbitals on iridium to form four M–CH_2 bonding orbitals (not shown for clarity) and four M–CH_2 antibonding orbitals. The $1a_1$ orbitals on the tantalum and iridium can then combine to form a M–M bonding orbital and a M–M antibonding orbital. The tantalum donates one electron and the iridium two electrons into these two orbitals. However, a half-filled iridium orbital lies lower in energy and subsequently becomes

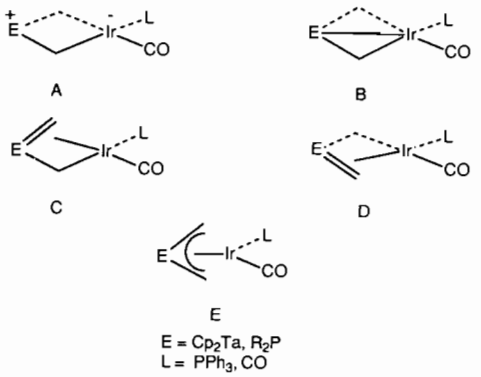

Fig. 10. Possible resonance structures for $Cp_2Ta(CH_2)_2Ir(CO)(L)$ and $R_2P(CH_2)_2Ir(CO)(L)$.

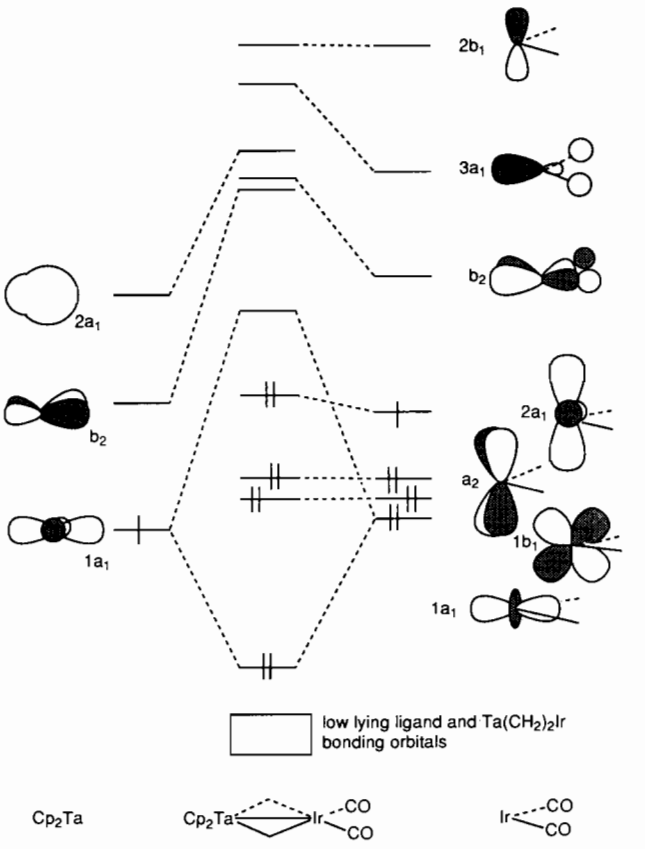

Fig. 11. Proposed molecular orbital diagram for $Cp_2Ta(CH_2)_2Ir(CO)_2$.

the filled HOMO (highest occupied molecular orbital). (The $2a_1$ orbital is usually assigned to be the HOMO for iridium(I) square-planar complexes.) The lowest unoccupied molecular orbital (LUMO) is proposed to be the M–M antibonding orbital; the LUMO for iridium(I) square-planar complexes is typically metal–ligand antibonding.

Spectroscopic properties

The electron density at iridium in the Ta–Ir and Ta–P complexes is similar when the iridium center is *four*-coordinate, as revealed by their nearly identical CO stretches in the IR spectrum for the PPh_3 complexes: **3**, 1934; **6a**, 1934; **6b**, 1929 cm^{-1} (C_6D_6). However, the ylide complexes exhibit lower-energy CO absorptions (i.e. the iridium center is more electron rich) when the Ir(I) center is *six*-coordinate, as in the methyl iodide oxidative addition compounds: **5b**, 2000; **8a**, 1986; **8b**, 1981 cm^{-1}. Thus, for four-coordinate complexes, the P–CH_2 group and the Ta–CH_2 group have a similar *trans* influence [27], whereas in higher coordinate complexes, the P–CH_2 group exhibits a stronger *trans* influence.

The UV–Vis bands for the Ta–Ir complex **3** appear at 389, 428 and 476 nm, whereas for the corresponding ylide complex **6a** the bands come at 367, 404 and 458 nm, ~22 nm higher in energy. This is consistent with the lower energy LUMO predicted for **3** from the MO diagrams. If the $R_2P(CH_2)_2^-$ and $Cp_2Ta(CH_2)_2^-$ fragments were bound to the Ir(CO)(L) fragment in the same manner, near identical UV–Vis absorbances might be predicted (since the electronegativities of the two fragments appear to be similar). This supports the idea that the fragments bind to the iridium center differently.

The ^1H and $^{13}C\{^1H\}$ NMR chemical shifts for the μ-CH_2 groups of the bimetallic complexes come at much lower field than for the ylide complexes. Consistent with the difference in bonding seen in the X-ray structures, the $[R_2P(CH_2)_2]^-$ group seems to coordinate to Ir in an alkyl-like fashion, whereas a more delocalized type of bonding is associated with the $Cp_2Ta(CH_2)_2Ir$ moiety.

Not predictable from the solid-state structures is the fact that the C–H coupling constants for the CH_2 groups on the ylide and Ta compounds are nearly identical. Typically, J(CH) is used to obtain an approximate idea of the type of hybridization present at carbon [28]. However, this is not necessarily applicable to organometallic compounds. For example, J(CH) is 132 Hz for the methylene carbon and 125 Hz for the methyl carbon in $Cp_2Ta(CH_2)(CH_3)$ [11]. Thus, it may not be advisable to compare directly the J(CH) value for our ylide and tantalum complexes. However, within each set of compounds, J(CH) is higher when the iridium center is formally in the +3 rather than the +1 oxidation state. This is consistent with the effect of changes in electronegativity on C–H coupling constants [28].

VT-NMR

As noted earlier, the NMR behavior of the TaIr–PEt_3 compound **2** is consistent with the rapid dissociation/association of the triethylphosphine ligand (Fig. 12). At low temperature, the ^1H NMR spectrum is consistent with a solution structure identical to that in the solid state. The solution fluxionality of the TaIr(dppe) compound **4**, in which the Ta–CH_2–Ir groups are equivalent above −75 °C, indicates the groups on the iridium center are exchanging sites. Because **4** does not decompose when rapidly stirred in an open vial (suggesting that rapid CO loss is unlikely), this exchange may be due to either Berry pseudorotation or dissociation of one of the phosphine arms (Fig. 13). We are unable to distinguish these processes at this time. The other phosphine-containing dinuclear compound $Cp_2Ta(CH_2)_2Ir(CO)(PPh_3)$ (**3**) appears to be static on the NMR time scale.

The ylide complexes **6a** and **6b** experience a different type of fluxionality. We believe that the puckered metallacycle undergoes ring inversion, but that this is a rapid process on the NMR time scale even at very low temperatures as evidenced by the equivalence of the ylide Ph or Me groups at all measured temperatures.

We believe that broadening of the PPh_3 peak in the $^{31}P\{^1H\}$ NMR spectrum of **6a** and **6b** is due to reversible dissociation of the PPh_3 ligand to form free triphenylphosphine and the three-coordinate iridium complex (Fig. 14). Thus, when PPh_3 is added to the NMR solution and the reaction is again monitored over the same temperature range, a resonance is seen halfway between the resonances for free PPh_3 and the bound phosphine. As the sample is cooled, this resonance

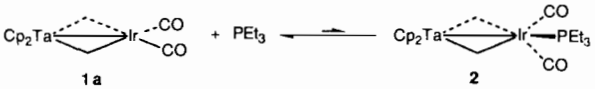

Fig. 12. Proposed mechanism for the observed fluxional behavior of $Cp_2Ta(CH_2)_2Ir(CO)_2(PEt_3)$ in THF-d_8.

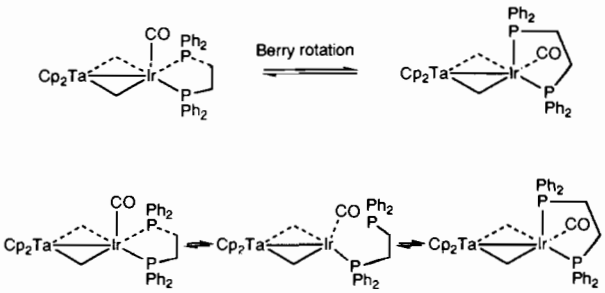

Fig. 13. Proposed mechanisms for the observed fluxional behavior of $Cp_2Ta(CH_2)_2Ir(CO)(dppe)$ in THF-d_8.

Fig. 14. Proposed mechanism for the observed fluxional behavior of $R_2P(CH_2)_2Ir(CO)(PPh_3)$ in THF-d_8.

disappears into the baseline and separate broadened signals appear at −109 °C, one of which corresponds to free PPh_3. Unfortunately the spectrum remains quite broadened at −109 °C, prohibiting any clear conclusion. However, if the fluxional process involved association of the PPh_3 to form a five-coordinate iridium center, we would expect, due to entropic considerations, that resonances corresponding to the five-coordinate species would dominate at low temperatures. This is not observed. The Rh analogue of **6a**, $Ph_2P(CH_2)_2Rh(CO)(PPh_3)$, is well behaved in solution in the presence of 1 equiv. of PPh_3. At low temperatures (−109 °C) the spectrum in THF-d_8 contains resonances for the ylide complex and free PPh_3. As the sample is warmed the resonances for free and bound phosphine broaden and then coalesce (−26 °C) at a chemical shift which is centered halfway between the free and bound resonances [24]. Interestingly, this dissociative behavior is seen only for the ylide complexes. The Ta–Ir–PPh_3 complex **3** is non-fluxional at all observed temperatures, and addition of free PPh_3 produces a spectrum consistent with the intermediacy of a five-coordinate iridium center.

It appears that the ELHB complexes are more stable toward ligand dissociation than the ylide complexes. One explanation may be that the CH_2 groups of the ylide fragment are better σ-donors (and thus have a stronger *trans* effect [27]) than the CH_2 groups of their tantalum analogue. Note that this trend is also seen for the *trans* influence.

Chemical reactivity

Although the Ta–Ir and P–Ir compounds undergo similar types of reactions, there are some differences in their quantitative reactivity. For example, only **6a** reacts with CH_2Cl_2 to form an isolable complex, whereas **1a** decomposes slowly in this solvent. However, the reaction with **6a** is exceedingly slow. In view of the complexity of some oxidative addition mechanisms, it is difficult to make a reliable reactivity comparison without further information on this reaction. In addition, the ylide dicarbonyl compounds $R_2P(CH_2)_2Ir(CO)_2$ could not be isolated. They can be detected by ^1H and $^{31}P\{^1H\}$ NMR spectrometry, but are over 50% decomposed within 1 day at room temperature in solution. The dicarbonyl ylide compounds were expected to be more stable than the monocarbonyl complexes since the iridium center formally has a negative charge associated with it and two π-acids should help to relieve this charge build-up. We currently do not have a good explanation for this observation.

TABLE 8. Rate data for the oxidative addition of methyl iodide to Ir(I) metal centers

Iridium complex	Conditions	k_{2nd} (M^{-1} s^{-1})
$Cp_2Ta(CH_2)_2Ir(CO)_2$ (**1**)[a]	THF, −5 °C	$6.83\pm0.34\times10^{-3}$
$Cp_2Ta(CH_2)_2Ir(CO)(PPh_3)$ (**3**)	THF, −5 °C	7.61 ± 0.43
$Ph_2P(CH_2)_2Ir(CO)(PPh_3)$ (**6a**)	THF, −5 °C	7.55 ± 0.30
$Me_2P(CH_2)_2Ir(CO)(PPh_3)$ (**6b**)	THF, −5 °C	17.9 ± 1.4
$MeIr(CO)(PPh_3)_2$[a]	THF, 0 °C	$2.26\pm0.05\times10^{-1}$
$PhIr(CO)(PPh_3)_2$[a]	THF, 0 °C	$2.12\pm0.05\times10^{-1}$
$ClIr(CO)(PPh_3)_2$[b]	DMF, 25 °C	2.8×10^{-2}

[a]Ref. 29. [b]Ref. 30.

To obtain a better feeling for the quantitative reactivity differences between the P–Ir and the Ta–Ir compounds, the reaction of MeI with **3**, **6a** and **6b** was examined. The rates for compounds **3** and **6a** are identical. At −5 °C, the second order rate constant for the oxidative addition of MeI to **3** was 7.61 ± 0.43 M^{-1} s^{-1} and the rate constant for **6a** was 7.55 ± 0.30 M^{-1} s^{-1} (Table 8). This suggests, as do the IR spectra of these materials, that the Ph_2P and Cp_2Ta moieties exert very similar electronic and steric influences at the Ir center. The more electron-rich and less sterically encumbered **6b** reacted more than twice as fast as the other two, with a second order rate constant of 17.9 ± 1.4 M^{-1} s^{-1}.

However, both the Ta–Ir and P–Ir compounds show increased reactivity when compared with other PPh_3 substituted iridium centers. For example, the rate for oxidative addition of MeI to $ClIr(CO)(PPh_3)_2$ is about 1000–2000 times slower; even the alkyl and aryl derivatives of Vaska's complex are at least 50–100 times less reactive. This enhanced reactivity may come from a major contribution from resonance structure A (Fig. 10), which predicts the iridium center to be highly nucleophilic due to its formal negative charge.The large rate difference between compounds **1a** and **3** probably stems from the replacement of a π-acid with a σ-donor.

Conclusions

The presence of a Ta–Ir metal–metal interaction is consistent with the X-ray structural data, the dynamic solution behavior and the spectroscopic characteristics of the compounds studied. This study has also shown that non-metal fragments can model certain aspects of transition metal fragments. The eventual goal of this work is to allow one to determine the effect of each transition metal on the overall properties of multimetallic complexes. However, there are still many perplexing comparisons which need further study.

Supplementary material

Details on the preparation of $CpCp^*Ta(CH_2)(CH_3)$, details on experimental protocol for the kinetic studies, a table of all measured rate constants, and representative $\ln(c/c_o)$ versus t plots (6 pages) are available from the authors upon request.

Acknowledgements

We would like to thank Johnson-Matthey-Aesar/Alfa for a generous loan of rhodium and iridium and the National Science Foundation for partial financial support of this work (Grant no. CHE-8722801).

References

1 D. W. Stephan, *Coord. Chem. Rev., 95* (1989) 41.
2 J. M. McFarland, M. R. Churchill, R. F. See, C. H. Lake and J. D. Atwood, *Organometallics, 10* (1991) 3530.
3 F. R. Lemke, D. J. Szalda and R. M. Bullock, *J. Am. Chem. Soc., 113* (1991) 8466.
4 F. Ozawa, J. W. Park, P. B. Mackenzie, W. P. Schaefer, L. M. Henling and R. H. Grubbs, *J. Am. Chem. Soc., 111* (1989) 1319.
5 C. P. Casey, F. R. Askham and L. M. Petrovich, *J. Organomet. Chem., 387* (1990) C31.
6 F. G. A. Stone, *Angew. Chem., Int. Ed. Engl., 23* (1984) 89.
7 L. Gelmini and D. W. Stephan, *Organometallics, 7* (1988) 849.
8 R. Choukroun, D. Gervais, J. Jaud, P. Kalck and R. Senocq, *Organometallics, 5* (1986) 67.
9 M. J. Hostetler and R. G. Bergman, *J. Am. Chem. Soc., 112* (1990) 8621.
10 M. J. Hostetler, M. D. Butts and R. G. Bergman, *Organometallics,* (1992) submitted for publication.
11 R. R. Schrock and P. R. Sharp, *J. Am. Chem. Soc., 100* (1978) 2389.
12 J. E. Baldwin and J. C. Swallow, *J. Org. Chem., 35* (1970) 3583.
13 D. R. Neithamer, R. E. LaPointe, R. A. Wheeler, D. S. Richeson, G. D. Van Duyne and P. T. Wolczanski, *Organometallics, 8* (1989) 1192.
14 T. Foo and R. G. Bergman, *Organometallics,* (1992) in press.
15 U. Klabunde, *Inorg. Synth., 15* (1974) 82.
16 P. Caddy, M. Green, E. O'Brien, L. E. Smart and P. Woodward, *J. Chem. Soc., Dalton Trans.,* (1980) 962.
17 J. R. Van Wazer, *Phosphorus and Its Compounds*, Interscience, New York, 1958.
18 F. A. Cotton and G. Wilkinson, *Advanced Inorganic Chemistry,* Wiley, New York, 4th edn., 1980, p. 467.
19 G. E. Ball, W. R. Cullen, M. D. Fryzuk, B. R. James and S. J. Rettig, *Organometallics, 10* (1991) 3767.
20 M. J. Hostetler and R. G. Bergman, *J. Am. Chem. Soc.,* (1992) submitted for publication.
21 E. N. Jacobsen, K. I. Goldberg and R. G. Bergman, *J. Am. Chem. Soc., 110* (1988) 3706.
22 T. V. Ashworth, J. A. K. Howard and F. G. A. Stone, *J. Chem. Soc., Dalton Trans.,* (1980) 1609.
23 J. M. O'Conner and C. P. Casey, *Chem. Rev., 87* (1987) 307.
24 M. D. Butts and R. G. Bergman, unpublished results.
25 C. E. Holloway and M. Melnik, *J. Organomet. Chem., 303* (1986) 39.
26 T. A. Albright, J. K. Burdett and M.-H. Whangbo, *Orbital Interactions in Chemistry,* Wiley, New York, 1985.
27 C. H. Langford and H. B. Gray, *Ligand Substitution Processes,* W. A. Benjamin, London, 1966.
28 D. J. Pasto and C. R. Johnson, *Laboratory Text for Organic Chemistry,* Prentice-Hall, Englewood Cliffs, NJ, 1979, p. 243.
29 M. J. Hostetler and R. G. Bergman, *J. Am. Chem. Soc., 114* (1992) 787.
30 J. Halpern and P. B. Chock, *J. Am. Chem. Soc., 88* (1966) 3511.